Department of the Navy
Bureau of Ordnance
Contract NOrd-9612

MEASUREMENTS OF LIFT COEFFICIENTS FOR A FAMILY OF CONICAL RING TAILS PLANING ON WATER

Russell Greengard

Hydrodynamics Laboratory
California Institute of Technology
Pasadena, California

Report No. E-12.9
August 4, 1952

J. P. O'Neill
Project Supervisor

Copy No. 61

MEASUREMENTS OF LIFT COEFFICIENTS FOR A FAMILY OF CONICAL RING TAILS PLANING ON WATER

Introduction

When it is expected that the afterbody of a projectile will plane on the free surface of an open cavity, the lift coefficient of the planing shape is of primary concern to the projectile design engineer. To provide basic data applicable to the design of an afterbody subject to such planing conditions, lift coefficients have been determined for a family of rings planing on a flat water surface. Changes in chord-diameter ratio and in flare angle were the model variables while angle of attack and submergence were varied during the course of the measurements of lift force.

In order to eliminate strut and afterbody configuration as a further necessary variable in the present tests, the models were supported from the top so as to minimize interference with the basic flow pattern produced by a simple ring. All ring edges were cut perpendicular to the ring axis and lap finished to a blunt and sharp cornered configuration that could be easily reproduced.

Photographs of typical test conditions are included in this report so that the proper flow configuration can be associated with various points on the plots of lift coefficient. With judicious selection from the graphs, and careful consideration of the flow pattern, it should be possible to gain insight into the lift forces that would act on a prototype ring tail whose shape is different from those tested during this investigation.

The Lift of Planing Rings

The rings tested during this series of measurements were all thin-shelled frustums of right circular cones with 4-in. outside diameter bases and the following total apex angles: 0° (cylindrical ring), $+15^{\circ}$ (cone base downstream), and -15° (cone base upstream). For each of the three cone angles, tests were made on models having both 1-in. and 2-in. chord lengths as measured along the axis of the cone. A uniform shell thickness of 0.065 in. was used for all rings in this series.

The model sizes indicated above and the test velocity of 23.7 fps were selected after some preliminary investigation of scale effects. The

short chord length allowed the tests to be free of Froude number effects when the model diameter was larger than that of the planing cylinders previously reported.[1]* It also might be expected that these sharp-edged rings are less subject to other scale effects than either cylinders or rings with a smooth hydrofoil section since the sharp edges provide a definite line of separation for certain parts of the flow. It should be recognized that the results are for the type of flow pattern obtained with the simple, sharp-edged rings. The tests were confined to this blunt, sharp-edged section in order to reduce the program and allow more time for investigation of the other model variables.

The planing conditions most likely to occur with a cavity-running missile were simulated by making lift measurements on each of the six model configurations at a number of angles of attack between 0° to 20° while varying the submergence to produce draft-diameter ratios up to 0.6. A drawing of a typical ring and test configuration giving the definition of symbols used is shown in Fig. 1.

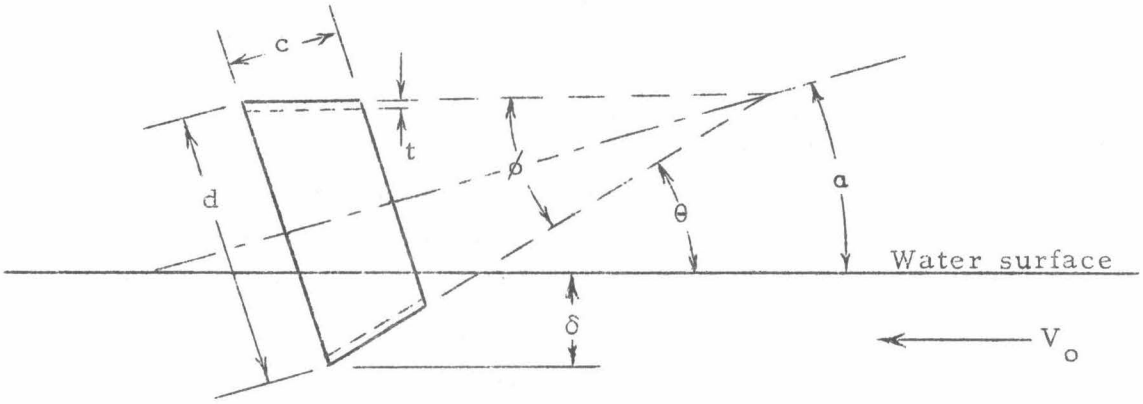

d = base diameter of model

δ = draft (submergence of lowest point on model)

c = chord length (measured along axis)

t = web thickness = .065

ϕ = total vertex angle of cone (ϕ<o when base upstream)

α = centerline of attack

θ = surface angle of attack = $\alpha + \frac{\phi}{2}$

ρ = mass density of water

V_o = free stream velocity

C_L = lift coefficient = $\frac{\text{lift force}}{1/2\rho V_o^2 d^2}$

g = gravitational acceleration

F_d = Froude number = $\frac{V_o}{\sqrt{gd}}$

Fig. 1 - Definitions of symbols

* See references at the end of this report.

The results of the lift measurements, plotted as lift coefficient against submergence with angle of attack as the variable, are given for the six model shapes in Figs. 2 to 7. All experimental points are included on these graphs except near the origin where only representative points are plotted to reduce crowding.

Two notable characteristics of the lift-coefficient curves are, first, the peaks of maximum lift coefficient which occur just after the leading edge of the ring is submerged and, second, the overlapping curves indicating double values of lift coefficient at some of the lower model positions. Careful observations of the flow pattern obtained for these various conditions have provided some explanation of the character of the curves.

It was observed that, when the leading edge of the rings was submerged, the water flowing through the ring separated at the inner corner of the blunt upstream edge and left the inner surface at the bottom of the ring open to the air. This condition held for all the test conditions except the few that were run at considerable negative surface angle of attack. Immediately after the leading edge of the ring is submerged, water is deflected so sharply upward that it impinges on the top inner surface of the ring and contributes to the lift. As the submergence is increased, however, the flow is deflected less sharply upward and it finally goes through the ring and misses the top inner surface. This is the most obvious factor contributing to the decrease in lift with increasing submergence; but further explanation based on the pressure distribution over the wetted portion of the ring is given in the discussion of results.

Another obvious change in flow pattern accounts for the existence of two values of lift coefficient at some of the high submergence ratios. At some submergence, depending on the model configuration and angle of attack, an air-ventilated cavity is formed on the outside bottom surface of the ring, thus altering the lift force. This outside air-ventilated cavity, once formed, is stable and changes little on further submergence of the model. A decrease in the submergence ratio below the value for cavity inception causes the cavity to disappear for large surface angles, while for small surface angles the cavity remains to produce two values of lift over a considerable range of submergence.

A knowledge of the flow patterns produced by the blunt, sharp-edged rings used in these tests is of considerable value when correlated with the

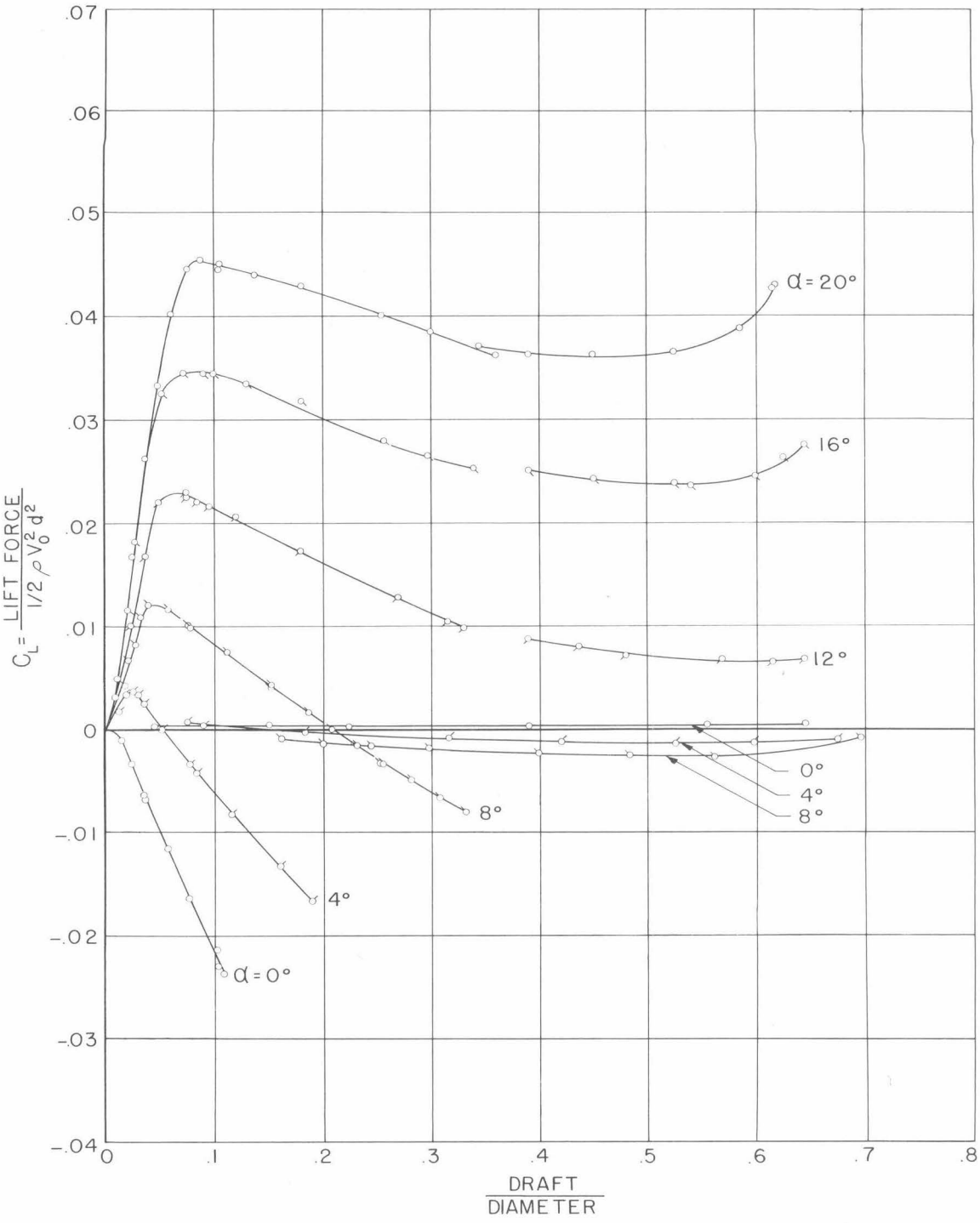

Fig. 2 - Lift coefficient vs draft-diameter ratio for a cylindrical ring planing on water at 23.7 fps and at various angles of attack α. Ring diameter 4 in., chord 1 in., thickness 0.065 in.

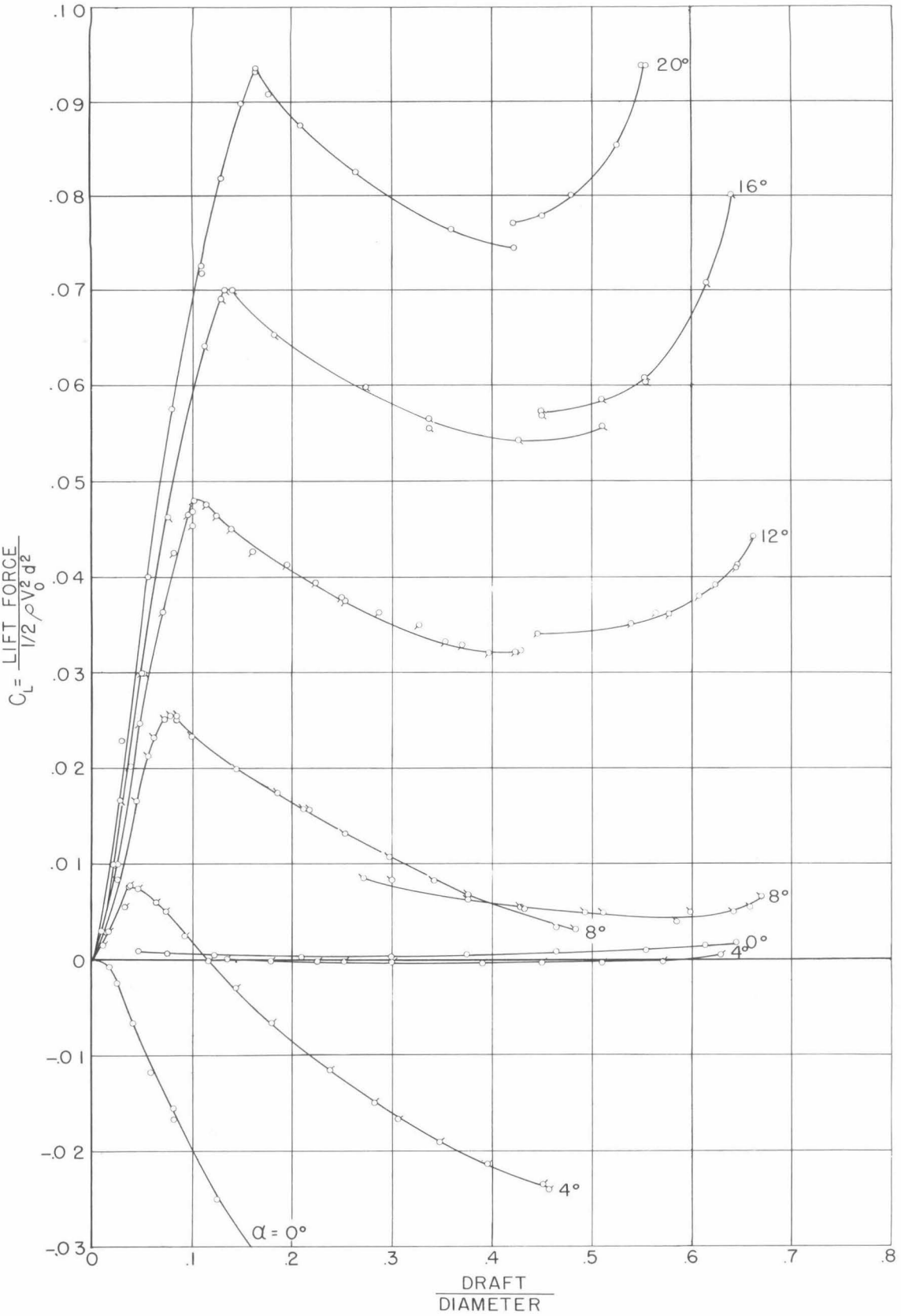

Fig. 3 - Lift coefficient vs draft-diameter ratio for a cylindrical ring planing on water at 23.7 fps and at various angles of attack α. Ring diameter 4 in., chord 2 in., thickness 0.065 in.

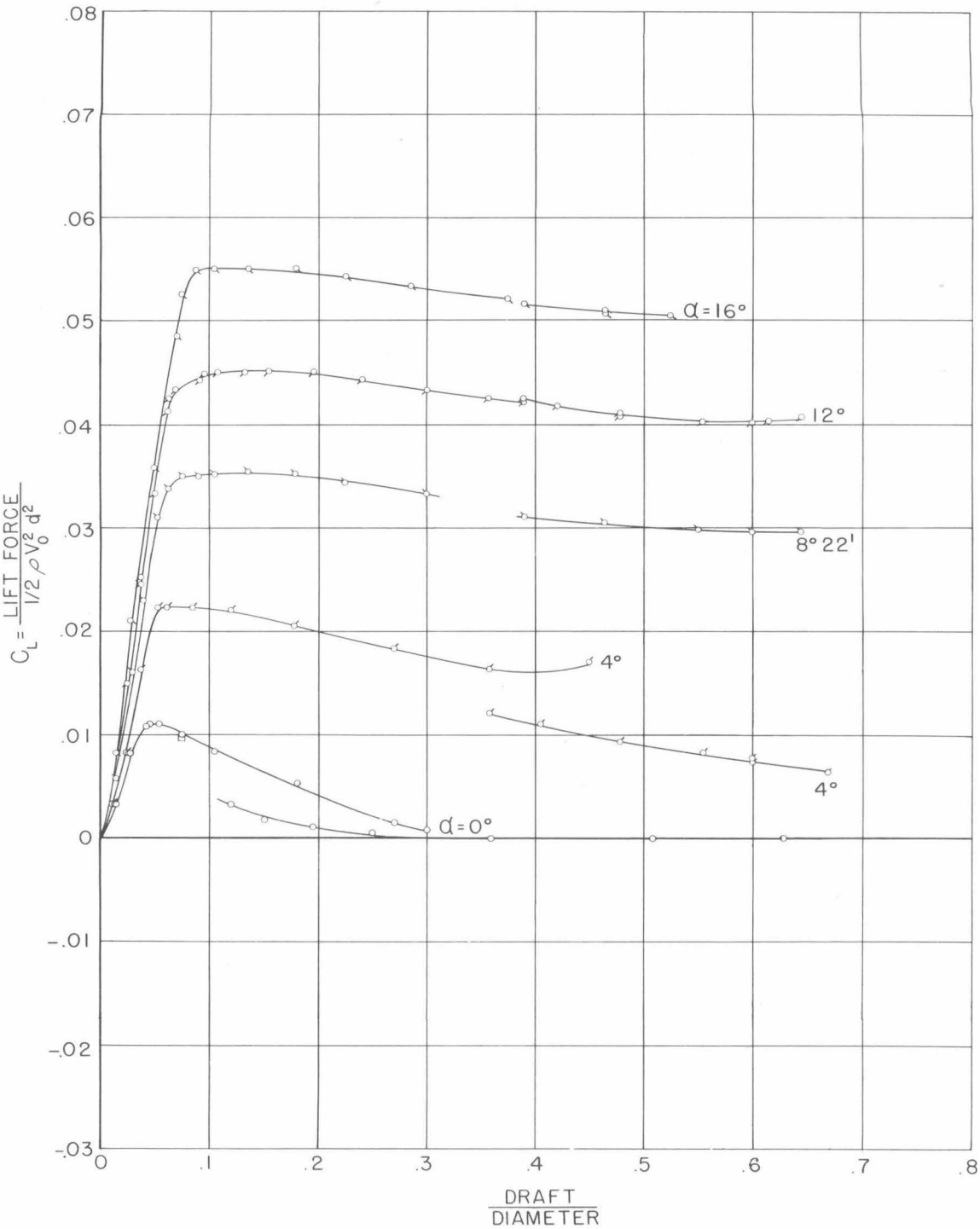

Fig. 4 - Lift coefficient vs draft-diameter ratio for a conical ring planing on water at 23.7 fps and at various angles of attack α. Total apex angle of cone $\phi = +15^{\circ}$ (base downstream); base diameter 4 in., chord 1 in., thickness 0.065 in.

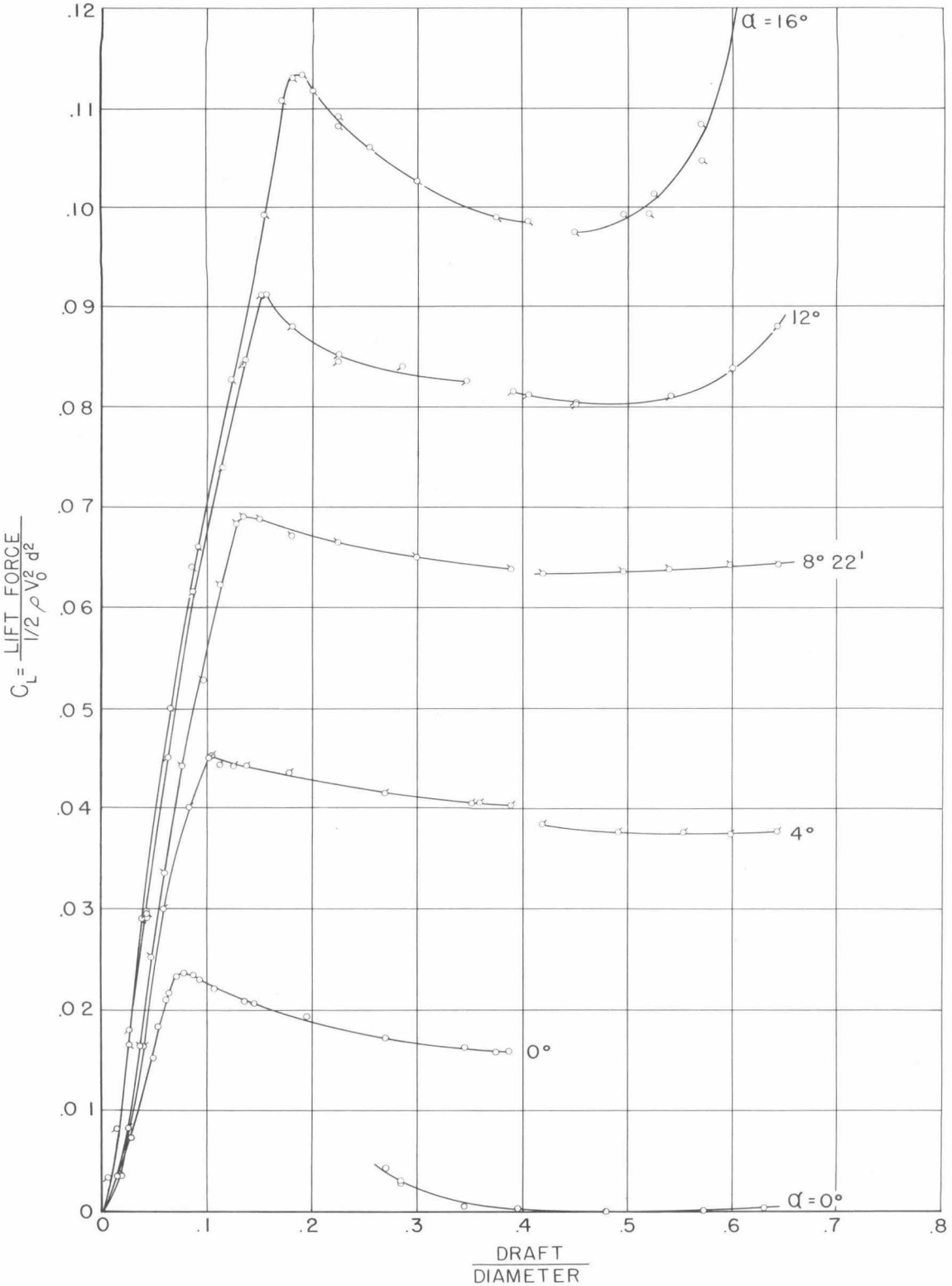

Fig. 5 - Lift coefficient vs draft-diameter ratio for a conical ring planing on water at 23.7 fps and at various angles of attack α. Total apex angle of cone ϕ = +15° (base downstream), base diameter 4 in., chord 2 in., thickness 0.065 in.

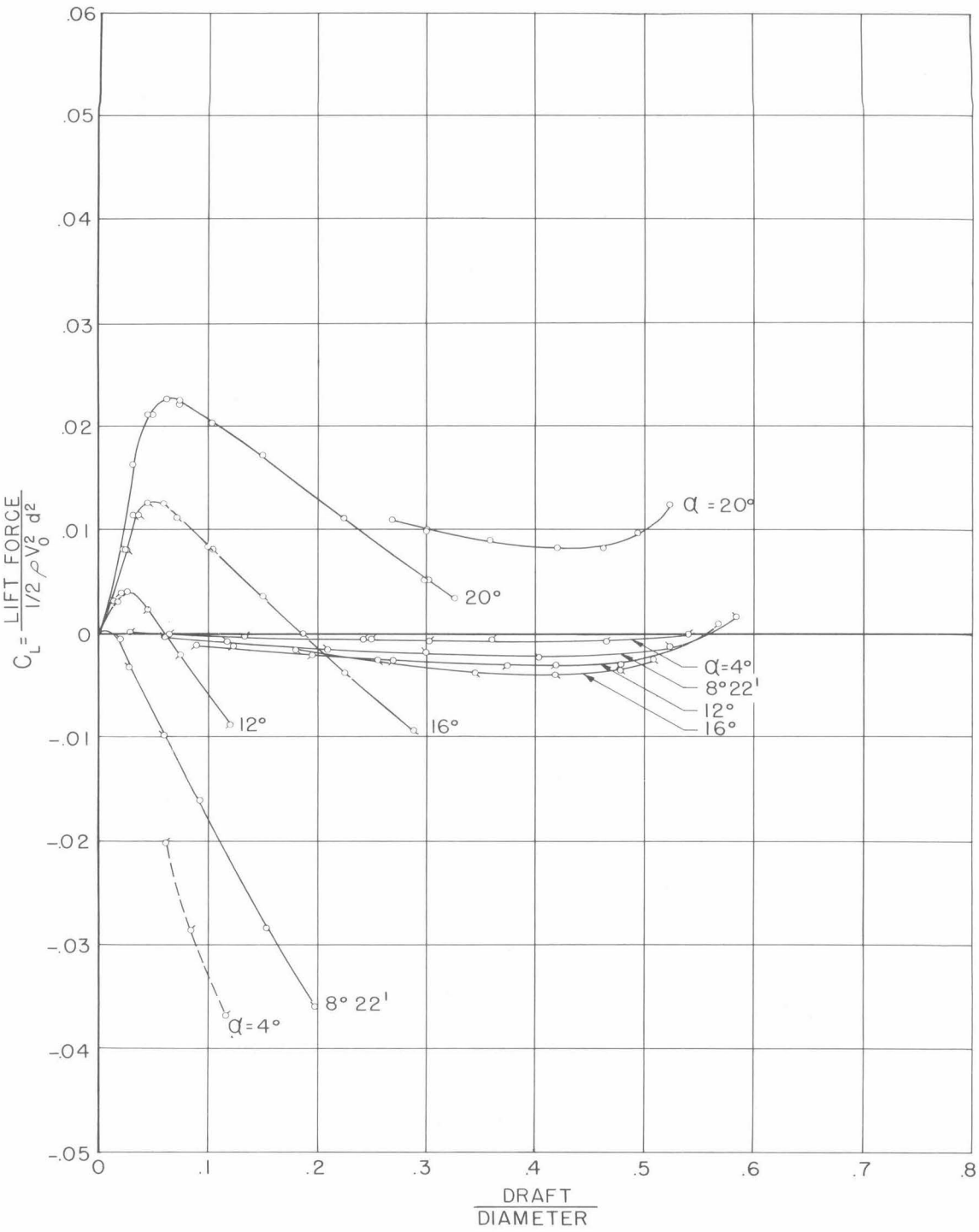

Fig. 6 - Lift coefficient vs draft-diameter ratio for a conical ring planing on water at 23.7 fps and at various angles of attack α. Total apex angle of cone ϕ = -15° (base upstream), base diameter 4 in., chord 1 in. thickness 0.065 in.

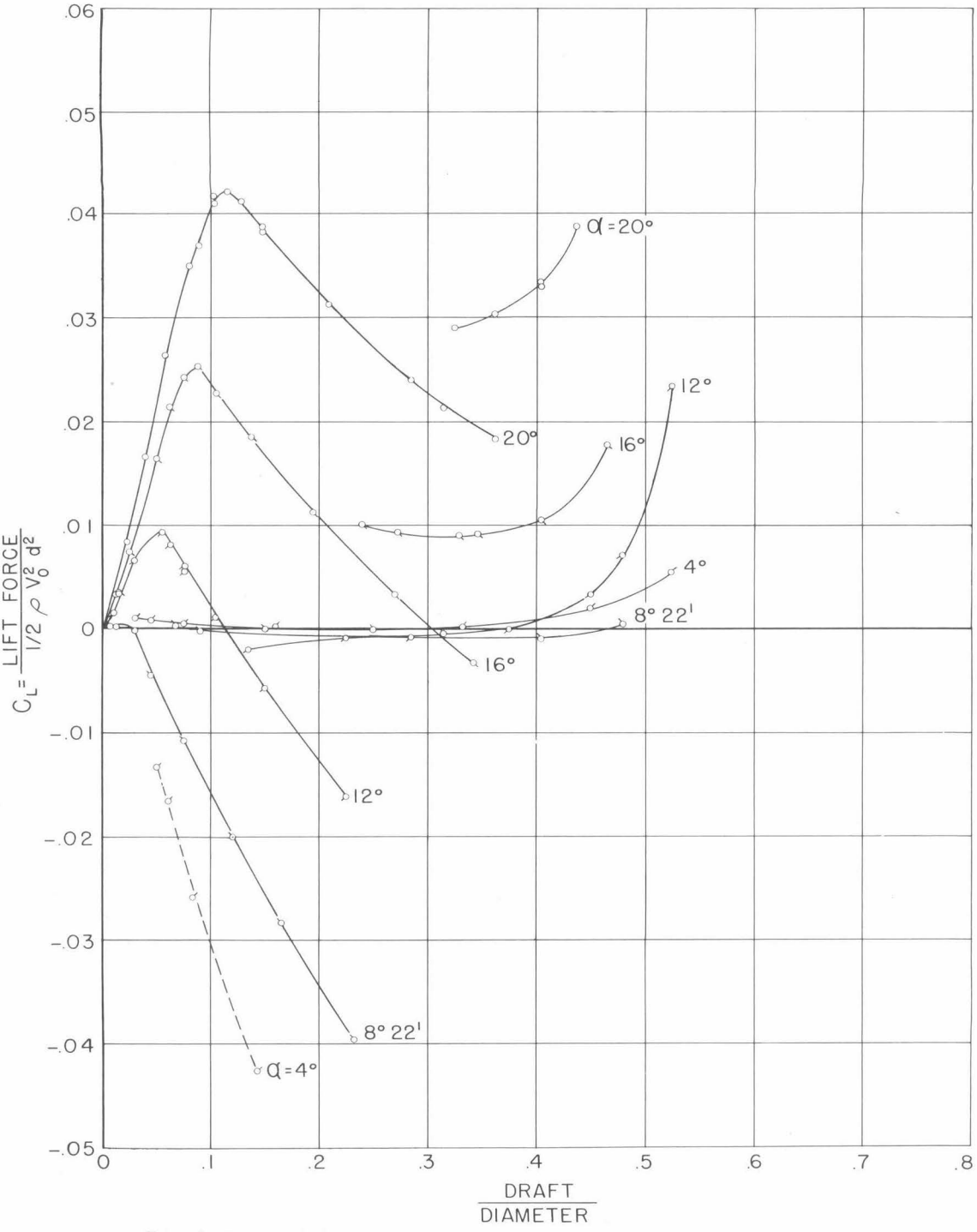

Fig. 7 - Lift coefficient vs draft-diameter ratio for a conical ring planing on water at 23.7 fps and at various angles of attack α. Total apex angle of cone $\phi = -15^{o}$ (base upstream), base diameter 4 in., chord 2 in., thickness 0.065 in.

lift-coefficient curves. Changes in the details of the ring construction should be examined for the expected changes in the flow pattern when comparisons with the present results are made. As an aid to such comparisons, further analysis of the present flow patterns is discussed below.

Discussion of Results

Until the lower leading edge of the ring tail becomes submerged, the flow pattern around the ring tail is similar to that which exists for the corresponding complete cone of "infinite" chord. Shown in Fig. 8 is a comparison of lift coefficients up to immersion of the leading edge for two of the ring models, with the results for the corresponding "infinite" chord cone models. The results, while similar, do differ slightly at these small submergences. This difference may be due to the action of the spray which flies off at the leading edge of the rings but clings and separates from a different point on the long cylinder and on the conical shape that is not truncated.

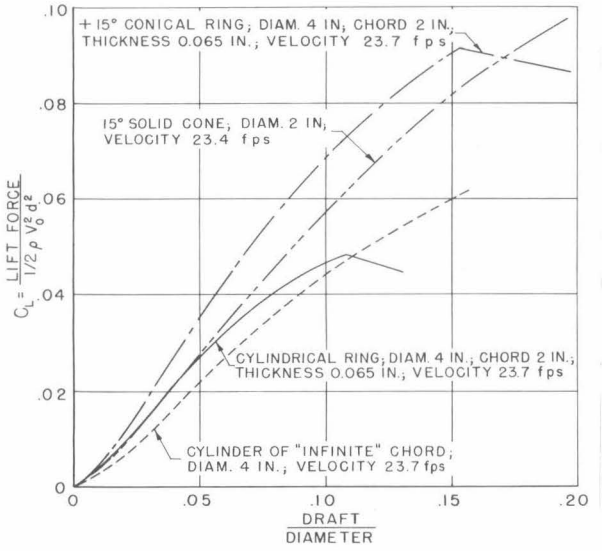

Fig. 8 - Comparison of lift coefficients for planing cylindrical and conical rings with the coefficients for the corresponding cylinder and cone of "infinite" chord. Angle of attack $\alpha = 12^{\circ}$.

It was previously reported[2] that complete cones of various apex angles produce approximately equal lift for the same surface angle of attack and submergence. This condition might also be expected for planing rings before the leading edge of the ring is submerged. Such a result is indicated in Fig. 9 which gives a comparison of lift coefficients for three rings of various apex angles at approximately equal surface angles of attack. That model surface angle of attack is not a good criterion for comparison between models of different apex angle once the leading edge becomes submerged is readily apparent.

The flow patterns associated with the different rings at equal surface angles of attack and at equal submergence prior to covering the leading edge are shown in Figs. 10, 11, and 12; Fig. 13 shows the same submergence of

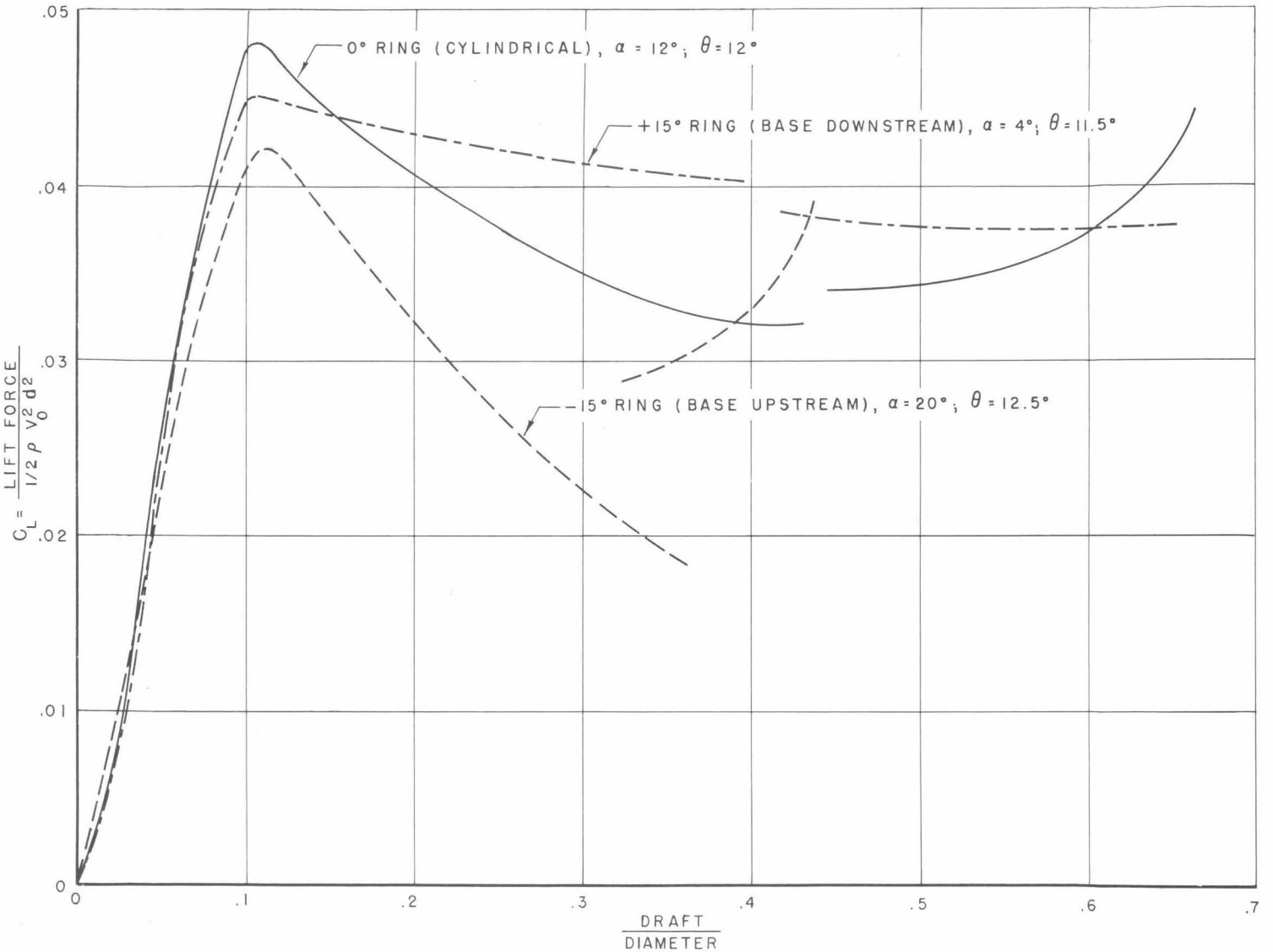

Fig. 9 - Comparison of lift coefficients for rings of various apex angles planing at 23.7 fps at various centerline angles of attack α but at approximately equal surface angles of attack θ. Ring diameter 4 in., chord 2 in., thickness 0.065 in.

CONFIDENTIAL

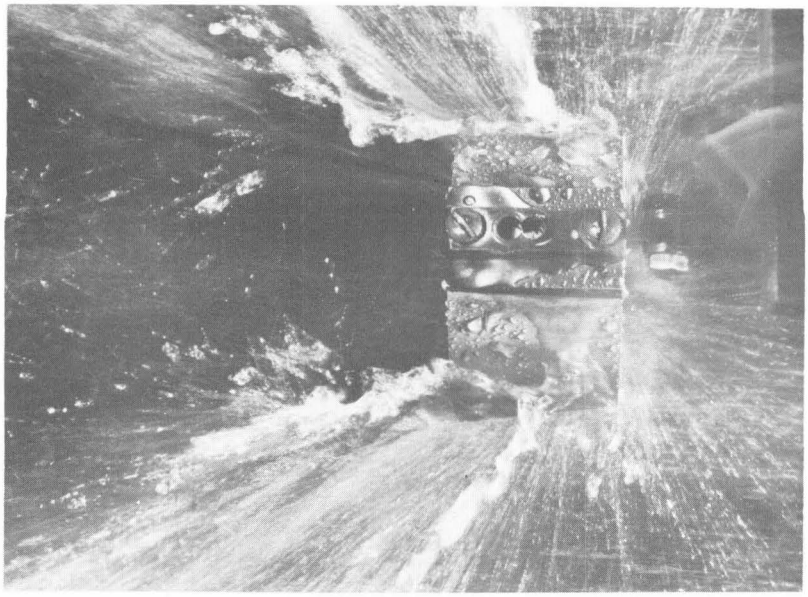

Fig. 10 - View looking down on a conical ring planing on a water surface with the base downstream. Water flows from right to left at 24 fps. Centerline angle of attack $\alpha = 4.5^{o}$; surface angle of attack $\theta = 12^{o}$; draft-diameter ratio = 0.07. Total apex angle $\phi = +15^{o}$; base diameter 4 in., chord 2 in., thickness 0.065 in.

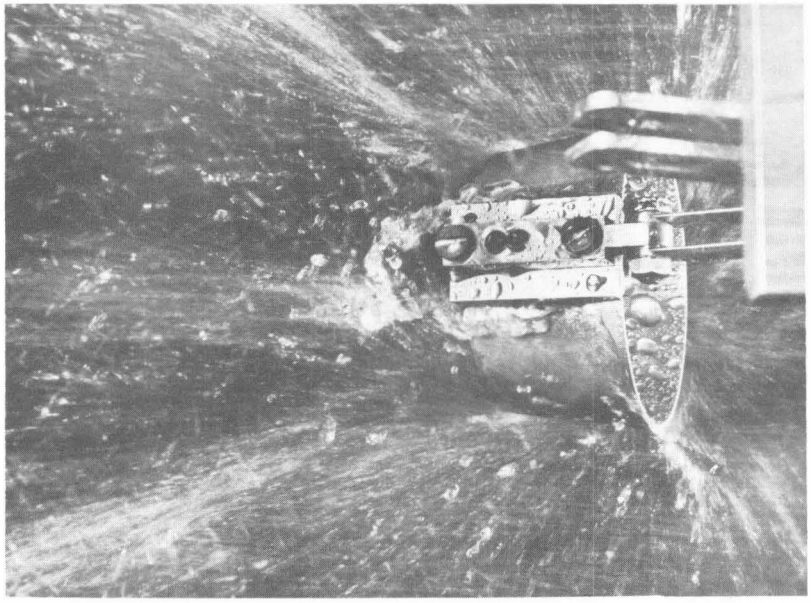

Fig. 11 - View looking down on a conical ring planing on a water surface with the base upstream. Water flows from right to left at 24 fps. Centerline angle of attack $\alpha = 19.5^{o}$, surface angle of attack $\theta = 12^{o}$, draft-diameter ratio = 0.07. Total apex angle $\phi = -15^{o}$, base diameter 4 in., chord 2 in., thickness 0.065 in.

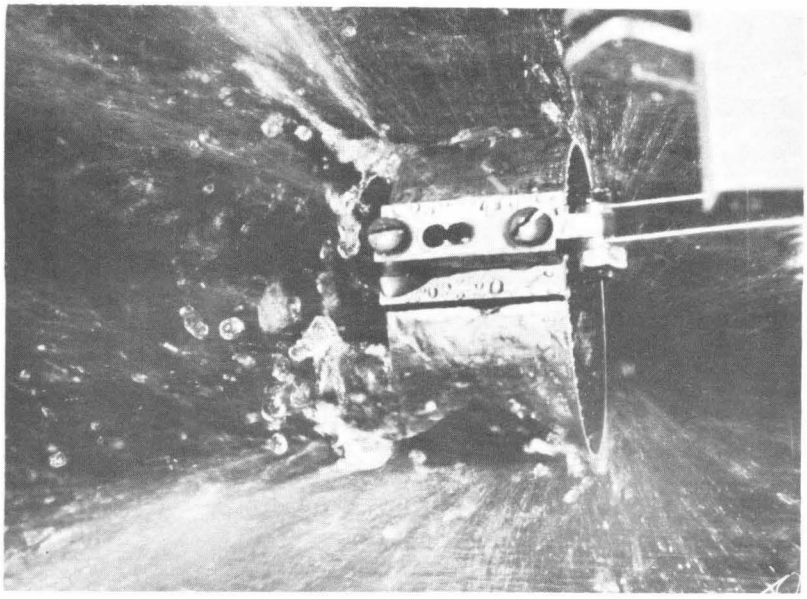

Fig. 12 - View looking down on a cylindrical ring planing on a water surface with the flow from right to left at 24 fps. Centerline and surface angle of attack = 12°, draft-diameter ratio = 0.07, ring diameter 4 in., chord 2 in., thickness 0.065 in.

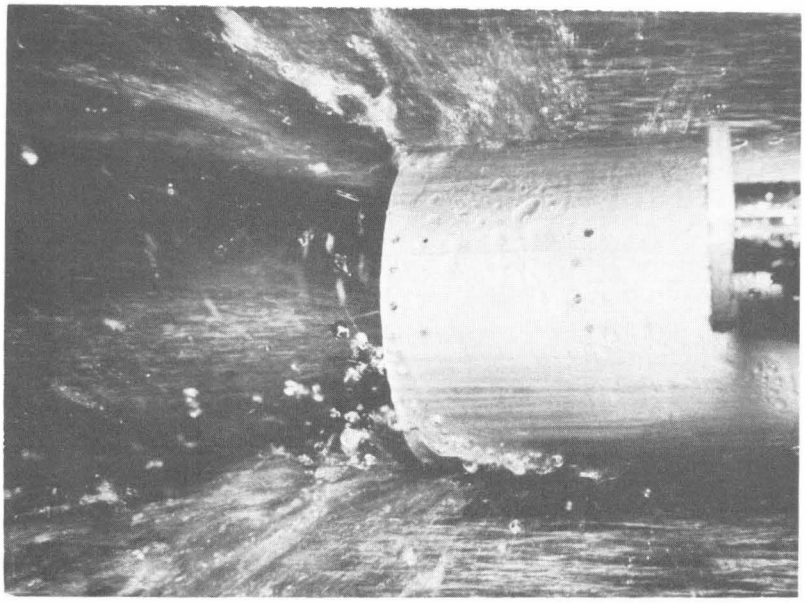

Fig. 13 - View looking down on a long cylinder planing on a water surface with the flow from right to left at 24 fps. Centerline and surface angle of attack = 12°, draft-diameter ratio = 0.07, diameter 4 in.

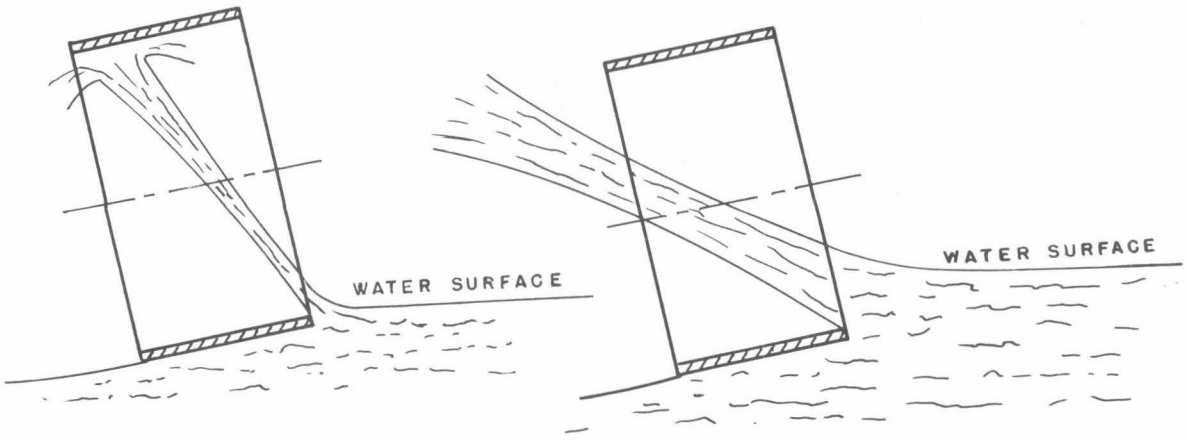

(A) At shallow submergence of the leading edge, flow sheet strikes inside top of ring.

(B) At greater submergence, flow through the ring is deflected less sharply upward so that it goes through the ring without striking the top.

Fig. 14 - Sketches of flow patterns at the center plane of a cylindrical ring planing on a water surface.

a cylinder of "infinite" chord. After submersion of the leading edge of the ring, the flow is different from that shown in these photographs primarily because there is some flow through the ring. As previously pointed out, this flow first strikes the top of the ring and then later, at deeper submergence, it goes through the ring without making contact with the top. The sketches of Fig. 14A, B depict this change in the direction of the flow through the ring as the submergence is increased.

It was observed that the distinguishing peaks in the lift-coefficient curves occur approximately at the submergence for which the leading edge first deflects considerable flow against the top of the ring. The effect of this impingement was investigated by deflecting the flow so that it no longer struck the ring, and noting the decrease in lift. Reductions as great as 12% were obtained depending on the size of this flow sheet and the amount its course was altered by the top of the ring. This portion of the lift is lost when the submergence is increased to the values where all the flow sheet goes through the ring without hitting the top. Even so, this effect does not appear to be sufficient to account for the magnitude of the decrease in lift on some of the models. Further contribution to the decrease in lift with increasing submergence might be due to the increase in the downward component caused by the pressure on the portion of the blunt front edge of the ring

subjected to near stagnation pressure. Furthermore, a zone of negative pressure exists on the outside bottom surface of the ring immediately behind the blunt leading edge. As the model submergence is increased, the domain of this negative pressure and its associated downward force spreads over a larger area.

The submergence for inception of the air-ventilated cavity on the outside bottom surface of the ring depends greatly on the model configuration and angle of attack. At some of the low surface angles of attack, however, there is also some dependence on how quickly the submergence is increased. Dashed lines on the lift coefficient curves in Figs. 6 and 7 indicate that the lift was obtained immediately after rapidly submerging to the indicated valves.

When the air-ventilated cavity forms over the outside bottom surface of the ring, the lift coefficient may increase, decrease, or remain constant depending on the surface angle of attack and the size of the cavity formed. For the higher surface angles only a small cavity forms which has negligible effect on the lift, while for surface angles less than about 8° the complete outside ring surface is sheathed in a cavity with the flow separating at the front edge of the ring. In Fig. 15 is shown a ring tail without an air-ventilated cavity, while in Fig. 16 is shown the same ring under the same conditions but with a cavity over a portion of the outside of the ring. The appearance of an air-ventilated cavity which completely covers the outside ring surface is depicted in Fig. 17. The nature of the cavity was similar for the 1- and 2-in. chord models at corresponding submergence conditions.

At the high angles of attack the slope of the lift coefficient curves increases rapidly after a submergence of about 0.5 is reached. This rapid increase in lift force is not the result of a change in the flow pattern around the outside of the model but is a consequence of the top surface of the ring coming into contact with the large flow through the ring. Such an increase might be expected to occur at a lower submergence for a prototype ring tail supported on fins that contact this flow sheet earlier in the course of an excursion into the wall of an open cavity.

Extension of Results to Prototypes

Scale effects on the sharp-edged planing rings were investigated at one representative angle of attack. The results, Fig. 18, indicate that any

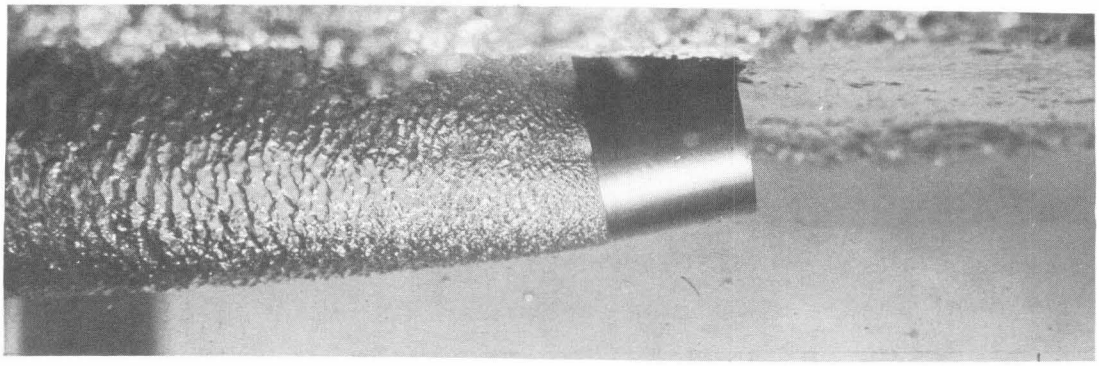

Fig. 15 - Underwater view of a cylindrical ring planing on a water surface with the flow from right to left at 24 fps. Angle of attack = 12°, draft-diameter ratio = 0.5, ring diameter 4 in., chord 2 in., thickness 0.065 in. On first approach to this submergence, no ventilation over the outside of the ring is observed.

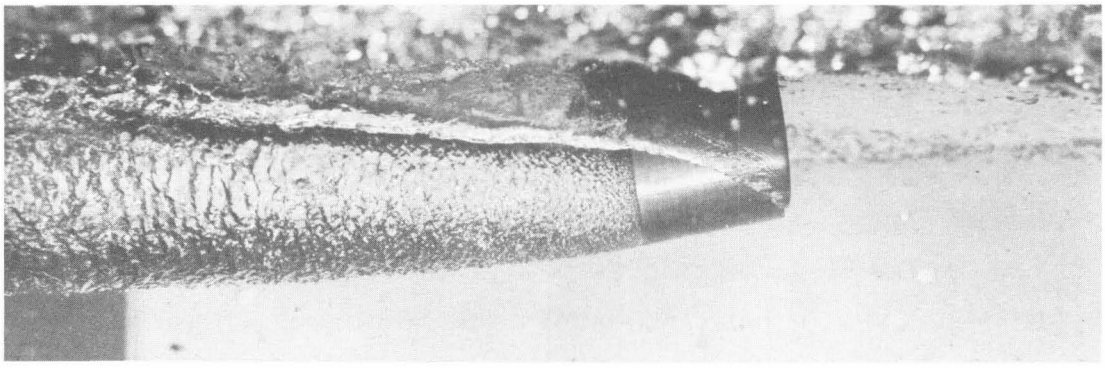

Fig. 16 - Underwater view for the same conditions as in Fig. 15 but showing alternate flow pattern after opening of an air-ventilated cavity over a portion of the outside surface of the ring.

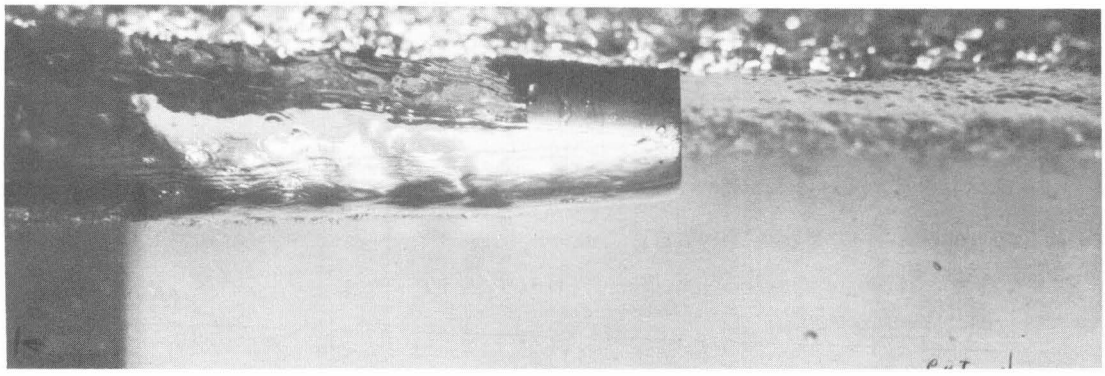

Fig. 17 - Underwater view of a cylindrical ring planing on a water surface at a smaller angle of attack than that shown in Figs. 15 and 16. Flow from right to left at 24 fps. Angle of attack = 4°, draft-diameter ratio = 0.4, ring diameter 4 in., chord 2 in., thickness 0.065 in.

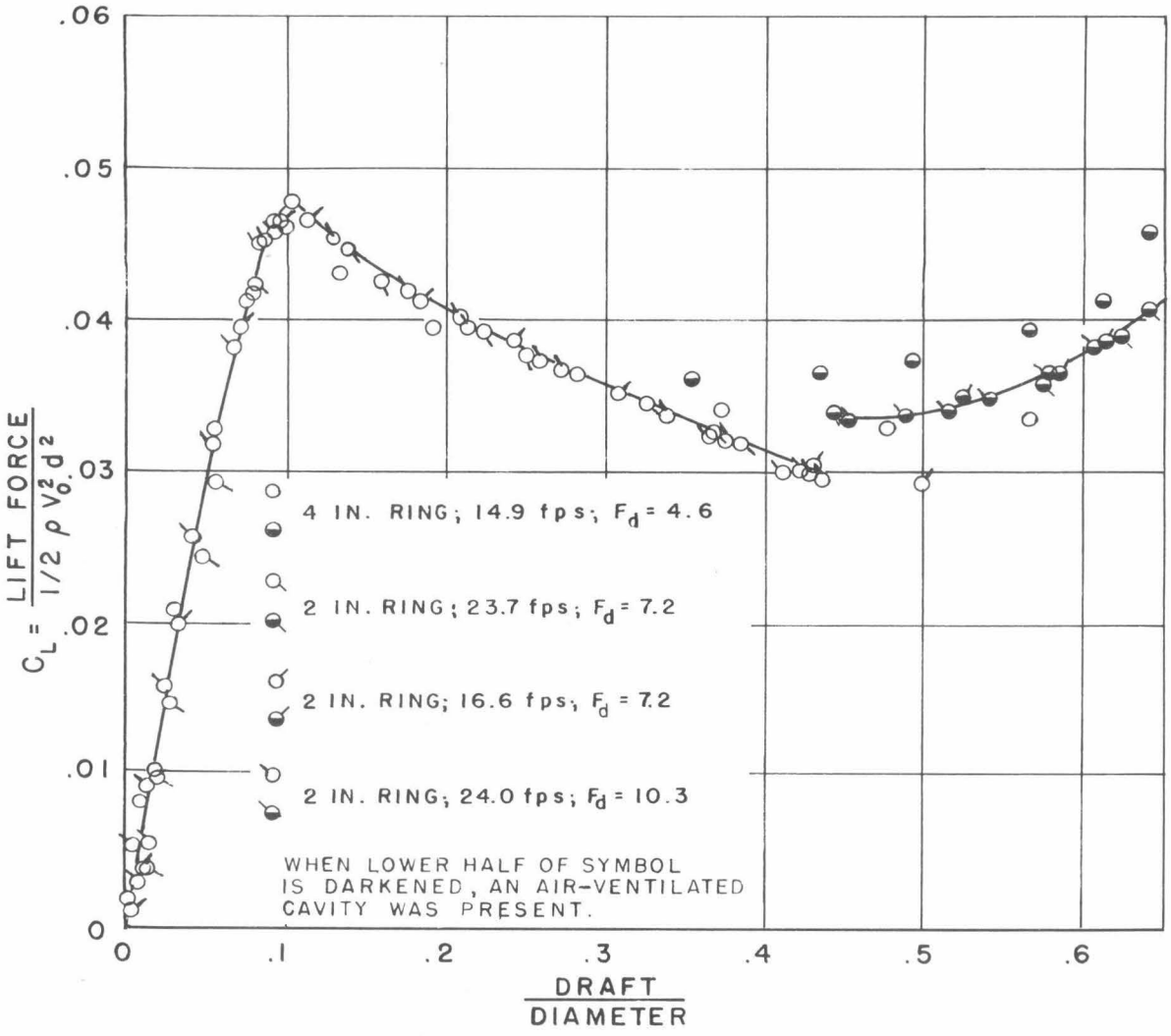

Fig. 18 - Lift measurements on geometrically similar models at different velocities indicate negligible scale effects for planing rings having a blunt, sharp-edged section. Test results shown are for cylindrical rings at 12° angle of attack. Rings of 4-in. diameter have a 2-in. chord and are 0.065 in. thick; 2-in. diameter rings have a 1-in. chord and are 0.032 in. thick.

scale effects in the submergence regions of greatest interest are negligible. It should be emphasized, however, that this result pertains to the sharp-edged series of rings chosen for these tests and that scale effects are more likely to occur with smoother shapes that do not have the separation points so well defined. Included in the tests plotted in Fig. 18 are the results for two cylindrical rings, one being an exact 1/2 scale model of the other. Runs for the two models were made at identical as well as at widely different

Froude numbers. The correspondence of results is excellent except in the air-ventilated cavity region where scale effects are present, but in this submergence region the support in prototype application would likely cause even greater discrepancies.

Various crossplots of the lift coefficient data may be made to indicate trends that are useful in the selection of a ring tail configuration. Fig. 19 is a representative comparison of the lift coefficients for all six blunt-edged rings at a constant centerline angle of attack of 8^{o}. The effect of variations in chord length or in apex angle is indicated by comparing the appropriate curves.

The basic shape used for the ring tail models precludes direct application of the results to a prototype except for those cases where use of a sharp, blunt ring edge is anticipated. For a ring with streamlined leading and trailing edges, the negative pressure region on the outside ring surface would be greatly modified, and the air-ventilated cavity is then less apt to form. In addition, with a smooth hydrofoil section, separation of the flow on the inside of the ring may not occur; and if it does, it probably would not start at the leading edge.

Careful consideration of the type of flow pattern to be expected from a prototype may lead to the establishment of useful approximations based on the present data. More precise estimates may require investigation of the effect of varying the ring cross section and the support system or possibly require tests of models of the specific afterbody designs under consideration.

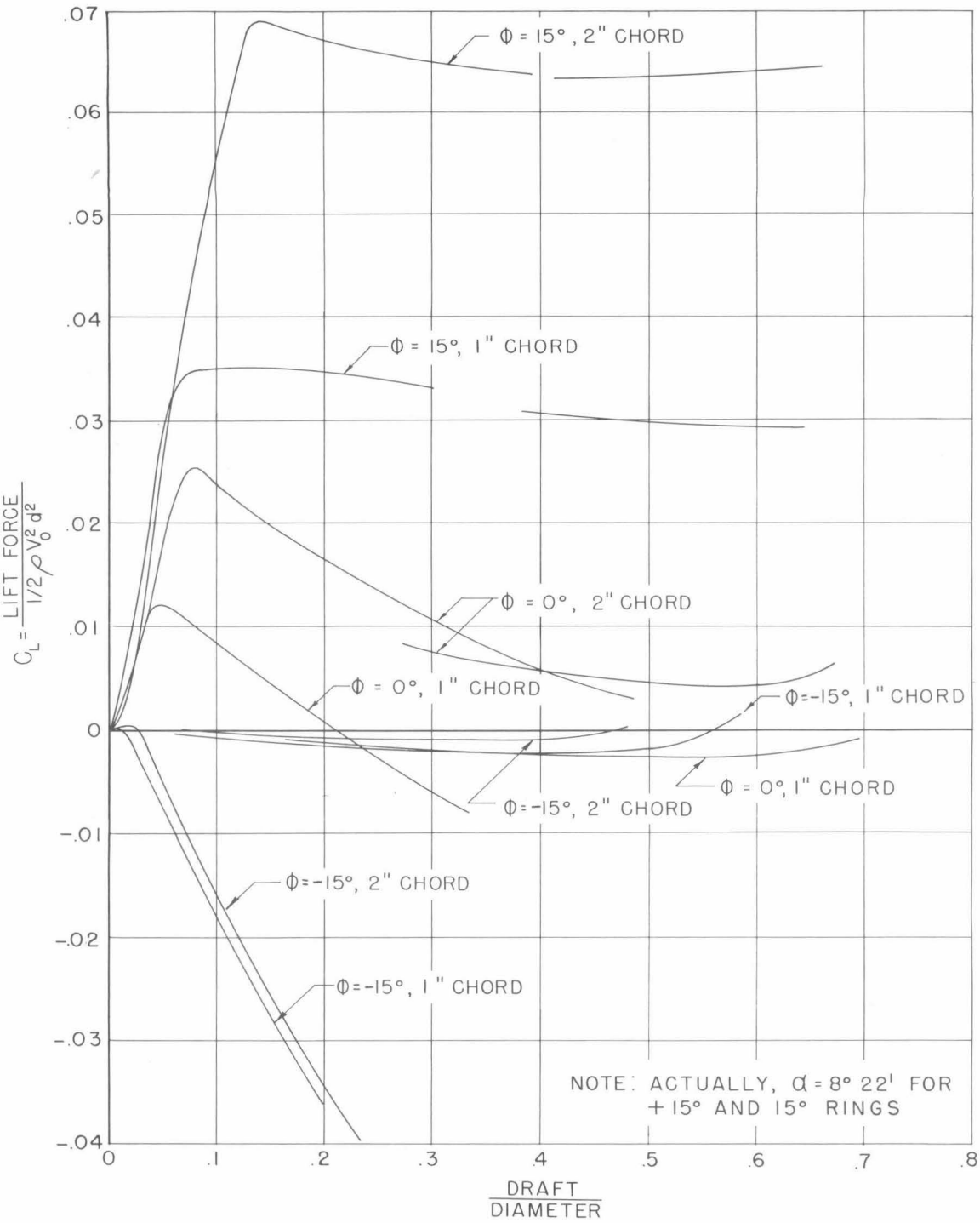

Fig. 19 - Lift coefficient vs draft-diameter ratio for cylindrical and conical rings planing on water at 23.7 fps showing effect of variation in apex angle and chord length. Angle of attack $\alpha = 8^{\circ}$, ring thickness 0.065 in.

APPENDIX

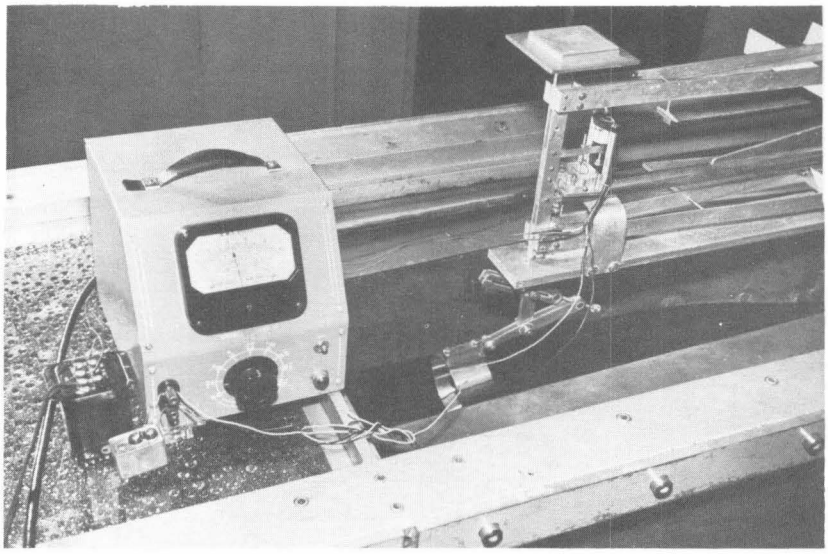

Fig. 20

Apparatus and Experimental Procedure

Figure 20 shows the single-component mechanical balance and its associated null indicating device used to measure the lift on the planing rings that were tested for this report. With the model mounted at the desired angle of attack, the model and balance were moved vertically into the flowing stream until the known load on the balance pan was just equalized by the lift force acting on the model. A counter, geared to the elevating device, measured the model submergence corresponding to this load. The null indicating apparatus consisted of a Schaevitz Linear Differential Transformer mounted on the balance with its output signal read by a voltmeter. A dashpot was used in conjunction with a steel spring to reduce balance oscillations resulting from tunnel turbulence, velocity variations, and water surface ripples. With this damping, the system was able to detect 0.002 lbs. The free movement of the model was limited by pins to $\pm$.025 in. and the amplification was set so that this motion gave full-scale deflection of the voltmeter. The spring constant was changed for the various models (spring constants of 2.5, 7.0, and 10.0 lbs/inch were used) to allow the voltmeter to read full scale under different unbalanced loads according to the oscillating component of the load which existed with each model.

The other experimental techniques and measurement errors for this report are similar to those discussed in Appendix I, "Apparatus and Experimental Procedure", of Ref. (2), and any necessary detailed information on procedure may be found therein.

BIBLIOGRAPHY

1. Kiceniuk, Taras, "Experimental Study of Froude Number Modeling for Cylinders Planing on Water", Hydrodynamics Laboratory, California Institute of Technology, Report No. E-24.4, January 7, 1952. (Restricted)

2. Kiceniuk, Taras and Greengard, Russell, "Measurements of Lift Coefficients for a Family of Cones Planing on Water", Hydrodynamics Laboratory, California Institute of Technology, Report No. E-12.3, January 7, 1952. (Confidential)

Department of the Navy
Bureau of Ordnance
Contract NOrd 9612

DISTRIBUTION LIST

Copy No.	
1	Chief, Bureau of Ordnance, Navy Dept., Washington, D.C. atten: Code Re6a
2	Chief, Bureau of Ordnance, Navy Dept., Washington, D.C. atten: Code Re3d
3-4	Chief, Bureau of Ordnance, Navy Dept., Washington, D.C. atten: Code Ad3
5-7	Chief, Bureau of Aeronautics, Navy Dept., Washington, D.C. atten: Code De3
8-12	Chief, Bureau of Ships, Navy Department, Washington 25, D.C.
13-15	Chief of the Office of Naval Research, Navy Dept., Washington, D.C., Code 438
16	Office of Naval Research, Los Angeles Branch, 1030 East Green Street, Pasadena, California
17-18	Director, David Taylor Model Basin, Washington 7, D.C.
19-20	Commanding Officer, Naval Torpedo Station, Newport, R.I.
21	Commander, Naval Ordnance Test Station, Inyokern, China Lake, California. Atten: Technical Library, Code 5507
22-23	Commander, Naval Ordnance Laboratory, White Oak, Silver Spring 19, Maryland
24-26	Officer-in-Charge, Pasadena Annex Naval Ordnance Test Station, Inyokern, 3202 East Foothill Blvd., Pasadena, California, atten: Pasadena Annex Library, Code P5507
27	Director, Experimental Towing Tank, Stevens Institute of Technology, via: Bureau of Aeronautics Representative, c/o Bendix Aviation Corp., Eclipse-Pioneer Division, Teterboro, New Jersey.
28	Director, Ordnance Research Laboratory, Pennsylvania State College, State College, Pennsylvania
29	Alden Hydraulic Laboratory, Worcester Polytechnic Institute, Worcester, Mass., via: Inspector of Naval Material, 495 Summer St., Boston 10, Mass.
30	Inspector of Naval Material, Development Contract Section, 1206 South Santee Street, Los Angeles, California
31-32	Superintendent, U.S. Navy Postgraduate School, Annapolis, Maryland.

Department of the Navy
Bureau of Ordnance
Contract NOrd 9612

Distribution List (Cont'd)

Copy No.	
33-34	Director, U.S. Naval Electronics Laboratory, Point Loma, San Diego, California
35-44	British Joint Services Mission, Navy Staff, via: Chief, Bureau of Ordnance, Navy Dept., Washington 25, D.C., atten: Code Ad8
45	Executive Secretary, Research and Development Board, National Defense Building, Washington, D.C.
46	Dr. E. Bromberg, Office of Naval Research, Mechanics Branch, Washington 25, D.C.
47	Commander, Submarine Development Group TWO, Box 70, U.S. Naval Submarine Base, New London, Conn.
48	Dr. F. C. Lindvall, 200 Throop, California Institute of Technology, Pasadena, California